SME Annual Meeting
Feb. 25 - 28, 2018, Minneapolis, MN

Preprint 18-075

CALIBRATION OF A COAL-MASS MODEL USING AN IN SITU COAL PILLAR STRENGTH STUDY

K. M. Mohamed, NIOSH, Pittsburgh, PA
G. Rashed, NIOSH, Pittsburgh, PA
M. M. Sears, NIOSH, Pittsburgh, PA
J. A. Rusnak, NIOSH, Pittsburgh, PA
M. A. Van Dyke, NIOSH, Pittsburgh, PA

ABSTRACT

Researchers from the National Institute for Occupational Safety and Health (NIOSH) recently developed a coal-mass model to realistically simulate the deformation and loading behaviors of the ribs of coal pillars in underground coal mines. The scale-dependent properties (stiffness and strength) of coal material were considered in the coal-mass model.

In this paper the orientation of face cleat with respect to driving direction was integrated in the coal-mass model. The controlling parameters (dimensionless coal-mass scale and fracture strains) of the modified coal-mass model were calibrated using a published case study of coal pillar strength.

Numerical models with wide ranges of controlling parameters were conducted to simulate the test pillar. The best match between the numerical modeling results and the measured stresses and deformations was achieved by using a coal-mass scale of 30 and fracture plastic shear and tensile strains of 3.25% and 0.325 %, respectively.

INTRODUCTION

The failure of coal pillar ribs by itself are a major hazard in underground coal mines. Furthermore, failing ribs can indirectly contribute to roof and floor instability by increasing opening widths across intersections and entryways. Over the past decade, rib failures have resulted in 12 fatalities, representing 28% of the ground-fall fatalities in U.S. underground coal mines. Mining depth has always played a very important role in assessing rib stability. Gauna and Mark (2010) completed an analysis of rib fatalities that occurred between 1996 and 2010. One of their most prominent and influential findings was the identification of a relationship among fatalities, depth, and mining height. Therefore, Coal rib stability will continue to be a challenge for future deeper mines in U.S. coal basins.

In the past several decades, research efforts have focused on roof support. The current rib control practice in U.S. coal mines is to select rib bolts through a trial-and-error approach (Mohamed et al., 2015a). Rib failure incidents can be can be substantially reduced or even eliminated by adopting an engineering-based coal rib design approach. The factors affecting rib stability in coal mines are numerous and mutually dependent. These factors include but not limited to mining height and overburden depth, interburden thickness for multiple-seam mining, coal strength, cleat density, entry direction with respect to cleat orientation, existence or absence of partings in the coal, percentage of extracted roof and/or floor rock, density of rib bolt support (Mohamed et al., 2015a). Moreover, it is difficult to isolate the particular effect of a specific factor on the overall rib stability. Therefore, a reliable empirical rib design approach is not achievable because it requires a significant number of case histories to be collected in order to have a reasonable range of all of the critical parameters. However, numerical modeling can be a practical tool to assist with rib support design if the modeling is realistic, which can only be achieved through calibration and validation of the numerical model against field data.

Mohamed et al. (2015b) developed a coal-mass model in which the peak strength of the coal material is evaluated by the generalized Hoek-Brown failure criterion (Hoek et al., 2002). The stiffness and strength of yielded coal material are degraded by the Fang and Harrison (2002) local degradation model. The dilation of the coal material is defined by the Alejano and Alonso (2005) peak-dilation model. Regression equations were developed for the coal scale-dependent parameters (peak and degraded) using testing results of laboratory coal samples and in situ small coal pillars.

The depth of rib fracture determines the optimum rib control technique; for instance, an optimum rib bolt length should be longer than the depth of the rib fracture. Therefore, Mohamed et al. (2016) modified the coal-mass model to simulate the development of rib fracture in coal material. The effect of rib fracture was simulated by imposing cohesion-less, ubiquitous joints for those elements that show plastic shear strain greater than calibrated fracture strains. A field-monitored site located within the travel road of a longwall panel in the Australian mine was used to define the fracture plastic shear strain. The best match between the modeling results and field-monitoring measurements (stresses and deformation in the test pillar) was obtained for a coal-mass size of 500 mm (20 in) and a fracture plastic shear strain of 2.75%.

Sears et al. (2017) calibrated the coal-mass model for the observed rib response of high pillar ribs in a bench room-and-pillar mining operation. The best match between the model response and field observations (depth of rib fracture) was obtained for a coal-mass size of 500 mm (20 in) and a fracture plastic shear strain of 3.0%.

Zhang et al. (2017) calibrated the coal-mass model for scoped rib fractures in a longwall coal mine in the Pittsburgh seam. Rib fractures were observed for various loading conditions throughout different mining cycles (gateroad development and longwall retreat). The best match between the numerically predicted rib fractures and rib scoping observations was obtained for a coal-mass size of 300 mm (12 in) and a fracture plastic shear strain of 3.0%.

Underground observations show that the rib stability depends on the relative orientation of the roadway with the strike direction of the face cleat. Under unfavorable roof and/or floor conditions, such as weak roof and floor heave, the cleat system in coal seams could promote rib sloughing. Rib stability problems are likely to occur when the angle between the roadway driving direction and face cleat orientation is less than 30 degree (Holmes, 1981). Face cleat orientation has the largest impact on rib performance during the development stage of mining, while during pillar extraction or longwall retreat its impact on rib performance is secondary (Colwell et al, 2005). In this paper, researchers from the National Institute for Occupational Safety and Health (NIOSH) continue to improve and calibrate the coal-mass model. The orientation of face cleat with respect to driving direction was integrated in the coal-mass model. The new model was made executable in the finite difference code FLAC3D as a user-defined constitutive model (ITASCA, 2017).

COAL-MASS MODEL

Mohamed et al. (2015b) developed a continuum coal-mass model to realistically simulate the loading and deformation mechanisms of coal pillar ribs. Regression equations were developed for peak and degraded coal-mass scale-dependent parameters using the testing results of laboratory coal samples and in situ testing of small coal pillars. The scaled parameters are given by the following equations:

$$m = 245 \times D^{-0.683} \quad \textit{Equation 1}$$

$$s = 267 \times D^{-1.359} \quad \textit{Equation 2}$$

$$\sigma_{cr} = 3,085 \times D^{-1.241} \quad \textit{Equation 3}$$

$$n_d = 0.144 \times ln(D) - 0.568 \quad \textit{Equation 4}$$

$$\gamma_{crit}^{ps} = 0.01 \times D^{0.44} \quad \textit{Equation 5}$$

where "m" and "s" are the Hoek-Brown peak strength parameters of the coal-mass model, "σ_{cr}" is the residual of the unconfined compressive strength, "n_d" is a Fang and Harrison degradation parameter, γ_{crit}^{ps} is the plastic shear strain that governs the rate of coal material degradation, and "D" is the coal-mass size in millimeters (mm). The range of coal sample sizes that have been used to develop the above regression equations was from 61 mm to 1.34 m (2.4 in to 4.5 ft). The coal-mass size "D" is a measure of the strength and stiffness of the coal material, i.e., stronger and stiffer coal material has a smaller coal-mass size. The definition of coal-mass size was ambiguous for some researchers. Therefore, a new dimensionless property called coal-mass scale (CMS) is introduced to replace the coal-mass size in the above equations. The coal-mass scale ranges from 1 to 100. The lower limit of the CMS represents a strong intact coal material, while the upper limit represents the weaker, in situ large scale of coal material. Equation 6 correlates the coal-mass size (D) and the coal-mass scale (CMS).

$$D = 48.081 + 12.919 \times CMS \quad \textit{Equation 6}$$

The equivalent coal-mass scale for former calibration studies ranges between 20 and 35, (Mohamed et al., 2016, Sears et al., 2017, Zhang et al., 2017).

In this paper, the coal-mass model was modified to introduce the effect of the orientation of face cleats on the behavior of coal ribs. The effect of face cleat was introduced through three assumptions: (1) the face cleats in coal ribs are planes of weakness, (2) the face cleats can be fractured in one of two modes, i.e. shear or tension, and (3) the orientation of the rib fractures coincide with the orientation of the face cleats.

The face cleat system in the coal model was simulated as smeared joints in coal material matrix. The strain-softening, ubiquitous joint model available in FLAC3D was modified to simulate the weakening effect of the smeared face cleat by introducing six additional material parameters: fracture plastic shear strain, fracture plastic tensile strain, joint friction angle, joint residual cohesion, joint residual tensile strength, and joint strength reduction rate. By default, the coal material is elastic or could be yielded but not fractured. Therefore, the default strength properties (cohesion, friction angle, and tensile strength) of the ubiquitous joints are assigned very high values. If the induced plastic shear strain in the coal material exceeds a predefined fracture shear strain, then the ubiquitous joints fracture in shear by reducing their cohesions and tensile strengths to the residual cohesion and residual tensile strength, respectively. The fractured joints become cohesion-less, i.e., the cohesion, and tensile strength of joints become zero, according to a predefined strength reduction rate. Otherwise, if the induced plastic tensile strain in the coal material exceeds a predefined fracture tensile strain, then the ubiquitous joints fractured in tension and became smooth, i.e., the cohesion, and tensile strength become zero and a very small friction angle is assumed.

The dip direction of the fractured joints will maintain their predefined dip direction while their dips will be redefined by the following equation:

$$\beta_j = 45^o \pm \frac{\varphi}{2}, for\ shear\ fractur$$

$$\beta_j = 90^o, for\ tensile\ fractur \quad \textit{Equation 7}$$

Where β_j is the angle between the normal of the fracture joint and the direction of maximum principal stress, and φ is the instantaneous friction angle of coal material.

In summary, the inputs required to define the coal-mass model can be categorized in two groups: group-1 comprises the properties of the coal-mass matrix (i.e., Young's modulus, Poisson's ratio, coal-mass scale and intact strength), and group-2 comprises the properties of the face cleat in the coal-mass model (i.e., orientation, fracture plastic shear strain, fracture plastic tensile strains, friction angle, and joint degradation rate for cohesion and tensile strength). Young's modulus, Poisson's ratio, and intact strength of the coal material can be obtained from uniaxial compression tests of laboratory coal samples. The other properties can be defined through calibration of the coal-mass model against field observations or measured stresses and deformations in coal ribs. In this paper, the controlling parameters of the coal-mass model (coal-mass scale and fracture strains) are calibrated using a published case of an instrumented pillar in the Keystone No. 1 mine , Wyoming and McDowell counties in southern West Virginia (Wang et al., 1976).

IN SITU COAL PILLAR STRENGTH STUDY

The calibration coal pillar strength study was conducted in the Keystone No. 1 Mine, WV. The mine produced coal from the Pocahontas No. 3 seam for 94 years until its closure in 1986. Wang et al. (1976) reported the results of two large-scale, in situ coal pillar strength tests at the mine. The test study panel, 5 Left off Harpers Valley Mains, was developed with five entries with pillars on 21 m (70 ft) centers and entry widths of 5.4 m (18 ft) (Figure 1). Panel dimensions were approximately 150 m x 540 m (500 ft x 1,800 ft) at the test study area. The barrier pillar between the 5 Left and 4 Left panel was initially designed to be 63-m (210-ft) wide. For the pillars (A and E) to be tested, the #1 entry was driven an additional 10 m (30 ft) into the barrier, resulting in a barrier width of 54 m (180 ft). Crosscut spacing was also increased, resulting in a 24-m (80-ft) square (rib-to-rib) test pillars. The average overburden depth at pillar A is 240 m (800 ft).

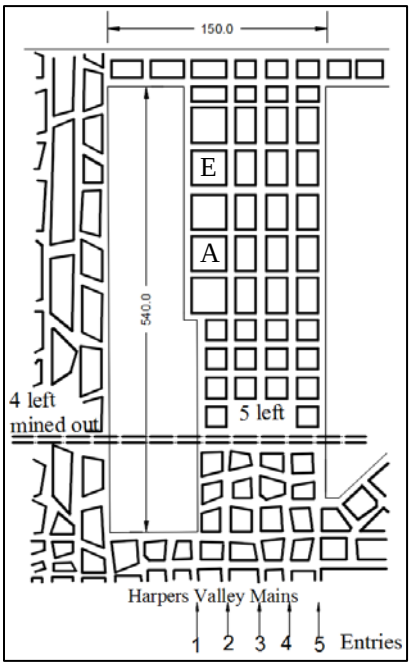

Figure 1. The test study panel (units are in meters). Reproduced after Wang et al. (1976).

The induced vertical stresses and rib deformations of the coal pillars were monitored, while the pillar was reduced in 17 cuts from 24 m x 24 m to 7.8 m x 7.8 m (80 ft x 80 ft to 26 ft x 26 ft). Figure 2 shows the first seven cuts in which the pillar was reduced to 18.6 m x 18.6 m (62 ft x 62 ft). The field test results for pillar E were not successfully obtained; therefore, only the field test results for pillar A will be used in the calibration of the coal-mass model.

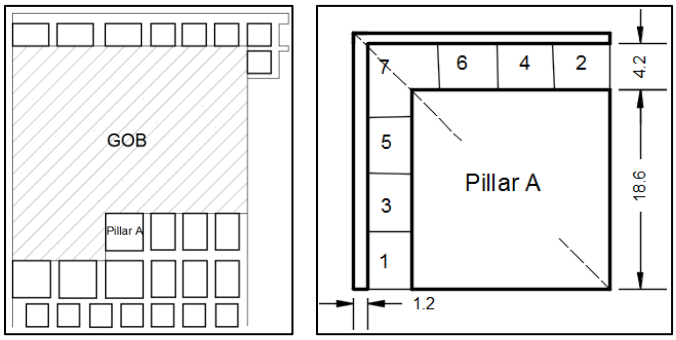

Figure 2. Pre-cut mining condition at instrumented pillar A (top) and pillar configuration after seven cuts were taken; units are in meters (bottom). Reproduced after Wang et al. (1976).

Changes in pillar stress were monitored throughout the loading cycle and the subsequent cross-section reduction experiment. To facilitate this, an array of vibrating wire stress meters (VWSM) were installed in a quarter of pillar A, prior to the #1 entry, and inby the crosscut isolating the pillar from the barrier, to monitor vertical stress changes throughout the subsequent process of pillar reduction (Figure 3). Stresses were reported for the pre-cut loading condition (Figure 2) and the subsequent final cuts at each pillar reduction, e.g. stresses were reported only for cut 7 when the pillar was reduced from 24 m x 24 m to 7.8 m x 7.8 m (80 ft x 80 ft to 26 ft x 26 ft).

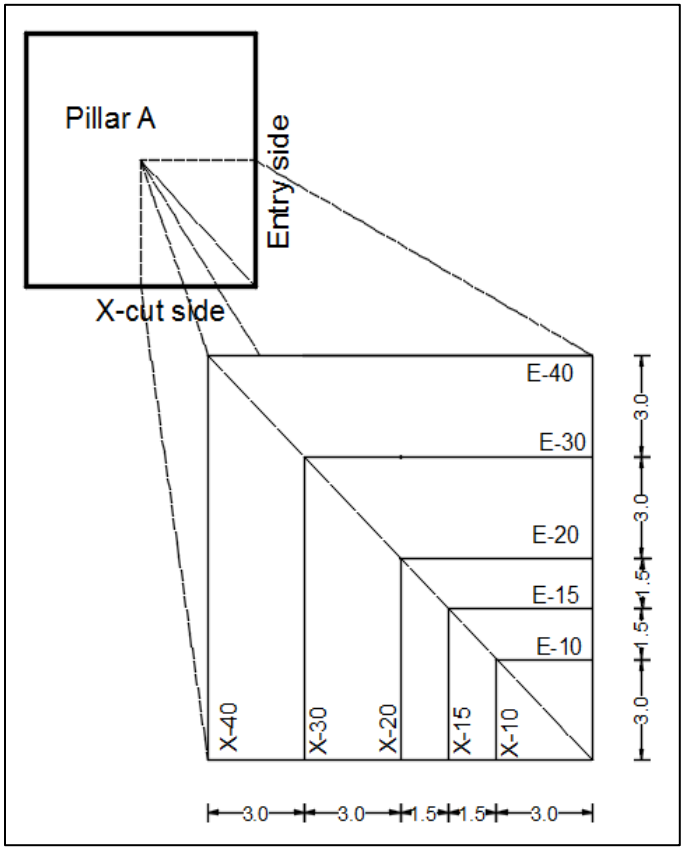

Figure 3. Location of stress meters in the instrumented pillar A (units are in meters). Reproduced after Wang et al. (1976).

Lateral rib displacement was measured using multi-point borehole extensometers (MPBX). An array of MPBXs were installed in a quarter of pillar A (Figure 4). VWSMs and MPBXs were installed 0.15 m (6 in) above and below the mid-height of the pillar, respectively. After the VWSMs were installed, they were monitored daily to ensure that the instruments were functioning properly and to obtain baseline readings. However, even though the MPBXs were in place, continuous logs could not be kept for these instruments. The amount of rib deformation of the MPBXs exceeded the working range of 25.4 mm (1 in). This is substantiated by the reported observation that after pillar extraction was begun, pillar ribs along the entries started to slough in the vicinity of the working face (Wang et al. 1976). This was particularly hazardous due to the volumes of material involved. While a definitive amount of displacement or rib sloughage is not reported, it does appear to be a significant amount. The rib anchors were repaired and reset prior to the cross-sectional area reduction experiment.

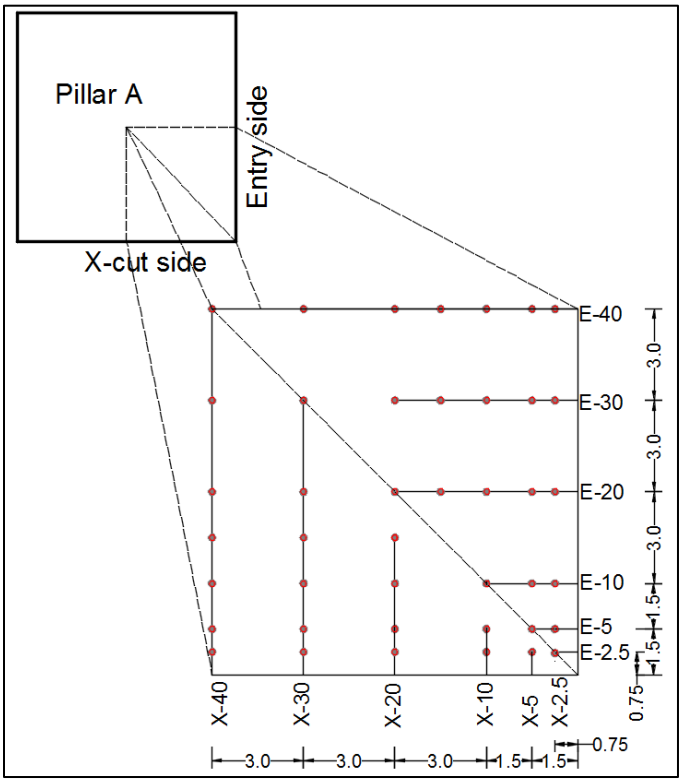

Figure 4. Location of rib deformation meters (MPBX) in the instrumented pillar A (units are in meters). Reproduced after Wang et al. (1976).

CALIBRATION OF THE COAL-MASS MODEL USING THE IN SITU COAL PILLAR STRENGTH STUDY

In this research, the calibration of the coal-mass model was conducted in the three steps described individually in this section; build FLAC3D models for the test site, define the geological and mechanical properties for the test site, and define the best match between the models and test site.

Step 1: Define the geological and mechanical properties for the test site

The reported average intact strength of the Pocahontas No. 3 seam at the test site is 13.2 MPa (1,914 psi), and the average Young's modulus and Poisson's ratio are 2.46 GPa ($3.56*10^6$ psi) and 0.25, respectively. The dip angle of face cleat is nearly 90 degree, and the strike of the face cleat is parallel to the entries at the test site. The immediate roof is 12 m (40 ft) of sandyshale overlain by 7.2 m (24 ft) of sandstone and the floor is shale at the test site. During the period of site monitoring, the immediate roof and floor were reported to be in good condition (Wang et al. 1976). Therefore, the roof and floor strata were assumed to be elastic. There were no reported rock testing data

for the roof and floor rocks. The mechanical properties for the roof and floor rocks were obtained from published data of similar rock types (Table 1).

The in situ horizontal stresses were not reported for the study site. The 5 Left panel, where the study was conducted, was driven in a SE-NW direction. The maximum horizontal stress in Eastern U.S. coal fields is generally orientated in an ENE-WSW direction. Therefore, the crosscuts at the study site were assumed to be oriented in the direction of the in situ maximum horizontal stress, and the entries were orientated in the direction of the in situ minimum horizontal stress.

The in situ horizontal stresses in rock strata for Eastern U.S. coal fields are calculated as follows (Esterhuizen, 2017):

$$\sigma_{Hr} = 0.313 + 0.027 * Z_r + .00278 * E_r \qquad \textit{Equation 8}$$

$$\sigma_{hr} = 0.65 * \sigma_{Hr} \qquad \textit{Equation 9}$$

Where σ_{Hr} and σ_{hr} are the maximum and horizontal stresses in MPa, respectively, E_r is the Young's modulus of rock strata in MPa, and Z_r is the depth of rock strata in meters.

The in situ horizontal stresses in the coal seam are calculated as follows (Liu, et al 2016):

$$\sigma_{Hc} = 1.174 + 0.024 * Z_c \qquad \textit{Equation 10}$$

$$\sigma_{hc} = 0.018 * Z_c - 1.475 \qquad \textit{Equation 11}$$

Where σ_{Hc} and σ_{hc} are the maximum and horizontal stresses in MPa, respectively, Z_c is the depth of coal seam in meters.

Step 2: Build FLAC3D models for the test site.

FLAC3D models were generated to simulate the size reduction process of the test pillar A (Figure 2). The lateral dimensions of the FLAC3D models were determined to ensure stress transfer between test pillar and surroundings; gob and pillars. The overall dimensions of the required FLAC3D model are 150 m x 150 m x 58.5 m (500 ft x 500 ft x 195 ft). The coal-mass model requires small elements, especially at the test pillar A, to realistically simulate rib fracture and deformation mechanisms. The element dimensions in the test pillar should not be greater than 0.3 m x 0.3 m x 0.3 m (1 ft x 1 ft x 1 ft). The number of required elements was found to be impractical for model size of 150 m x 150 m x 59.5 m (500 ft x 500 ft x 198 ft). Therefore, a global-submodel technique was used in this study. The global model is an elastic large model with a relatively coarse mesh. The global model was used to generate the required boundary conditions that can be applied on a smaller non-linear yieldable model (submodel) of finer mesh (Figure 5).

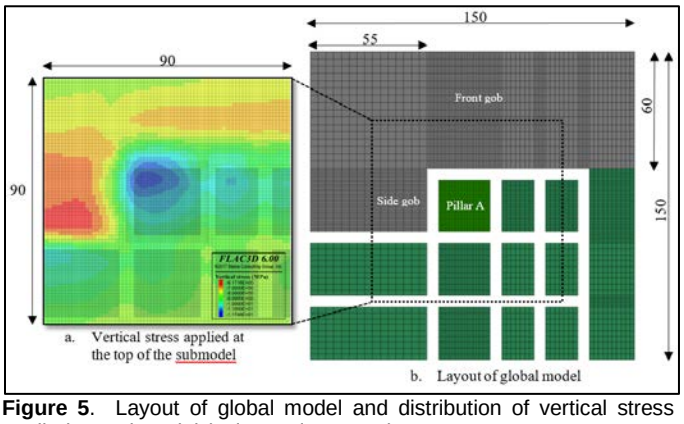

Figure 5. Layout of global model and distribution of vertical stress applied on submodel (units are in meters).

In the global model, the roof of 42 m (140 ft) was simulated by 21 rock layers to realistically transfer the load between the gob and coal pillars. The floor is simulated as a single layer 16 m (53 ft) thick. The model's bottom and its four sides are constrained by roller supports. A uniform pressure of 5 MPa (726 psi) was applied on the top of the global model. Table 1 summarizes the rock mechanics and interface properties used in the global model.

The gob height is assumed to be three times the mining height. The constitutive behavior of the gob material is expressed by strain-hardening behavior in the following equation (Salamon, 1990):

$$\sigma = \frac{E_o \times \varepsilon}{1 - \frac{\varepsilon}{\varepsilon_m}} \qquad \textit{Equation 12}$$

where:

σ = vertical gob stress.
E_o = initial Young's modulus of 10.61 MPa (1538 psi).
ε = vertical gob strain.
ε_m = maximum gob strain of 0.33.

The global model was solved in four steps: geostatic step, development of entries and crosscuts, front abutment loading, and side abutment loading. In the geostatic step, the in situ stresses were initialized in the model. In the development step, entries and crosscuts were developed. In the front abutment loading step, the pillars inby the test pillar A and caving zone were extracted and replaced by gob material. Similarly, in the side abutment loading step, the barrier to the left of test pillar A and caving zone were extracted and replaced by gob material. The vertical stress distribution at a distance of 15 m (50 ft) above the coal seam was exported from the global model (Figure 5a). The non-uniform vertical stresses obtained from the global model will be applied on the top of the submodel prior the pillar reduction step.

The dimensions of the submodel were 90 m x 90 m x 31.5 m (300 ft x 300 ft x 105 ft). The roof and floor are simulated as elastic layers of 15 m (50 ft). The coal seam thickness is 1.5m (5ft). The bottom and the four sides of the submodel were constrained by roller supports. The mechanical properties of the roof and floor layers are the same for the global model (Table 1). The coal and the coal/rock interface properties of the submodel are listed in Table 2. The coal-mass scale, the fracture plastic shear strain, the fracture plastic tensile strain, and the coal/rock interface friction were varied.

Table 1. Input parameters for global model.

Rock properties		
Rock type	Young's Modulus, GPa	Poisson's ratio
Coal	2.46 (3.56*10^5 psi)	0.25
Sandyshale	7.0 (1.02*10^6 psi)	0.26
Interface properties		
Friction, degree	15	
Cohesion, MPa	0.5 (72.5 psi)	
Tensile strength, MPa	0.3 (43.5 psi)	
Normal stiffness, GPa/m	150(6*10^5 psi/in)	
Shear stiffness, GPa/m	75 (3*10^5 psi/in)	

Table 2. Input parameters for submodel.

Coal-mass properties	
Young's Modulus, GPa	2.46 (3.56*10^5 psi)
Poisson's ratio	0.25
Intact compressive strength, MPa	13.2 (1914 psi)
Coal-mass scale	10 – 40*
Fracture plastic shear strain	0.025 - 0.055*
Fracture plastic tensile strain	0.0025 - 0.0055*
Joint friction angle, degrees	25
Joint residual cohesion, MPa	0.1 (14.5 psi)
Joint residual tensile strength, MPa	0.01(1.45 psi)
Joint degradation rate, MPa/strain	0.01(1.15 psi/strain)
Coal/rock interface properties	
Friction, degree	8.5 – 15*
Cohesion, MPa	0.3 (43.5 psi)
Residual cohesion, MPa	0.03
Normal stiffness, GPa/m	150 (6*10^5 psi/in)
Shear stiffness, GPa/m	75 (3*10^5 psi/in)

* Property range

The submodel was solved in four steps: geostatic step, entry and crosscut development, abutment loading, and pillar reduction. A uniform pressure of 5.59 MPa (811 psi) was applied on the top of the submodel during the geostatic and entry development steps. For the

subsequent steps, the vertical stress distribution imported from the fourth step of the global model (Figure 5a) was applied at the top of the submodel. In the pillar reduction step, the size reduction process of the test pillar was conducted in seven substeps (Figure 2).

Step 3: Define the best match between the models and test site.

A number of submodels for the test pillar A were created to simulate a wide range of modeling parameters (dimensionless coal-mass scale, fracture strains, and coal/rock interface). The coal-mass scale was varied in three levels—20, 30, and 40. The fracture plastic shear strain was also varied in three levels—0.0275, 0.0375, and 0.055. The fracture plastic tensile strain was one-tenth of the fracture plastic shear strain for all sub-models. The coal/rock interface angle was also varied in three levels—8.5°, 11.5°, and 15°. The modeling results (stress and displacement) of the test pillar A were extracted for three modeling steps: development, pre-cut, and cut-7 of pillar size reduction. The modeling results were compared with the field measurements (rib displacement, and vertical stress) of the test pillar. The best match between the model and field were found to be for a coal-mass scale of 30, fracture plastic shear strain of 3.75%, fracture plastic tensile strain of 0.375% and coal/rock interface angle of 11.5°.

Only, the modeling results of the submodel of the best match with the field measurements are presented in this paper. To study the anisotropic effect of the face cleat on the rib behavior, the submodel results was compared with the field measurements using two sets of profiles; i.e. entry side and crosscut side profiles (Figures 3 and 4). The entry side profiles are perpendicular to the face cleat, and the crosscut profiles are parallel to the face cleat at the test site. Profiles X-2.5, X-10, X-20, and X-30 were taken at distances of 0.75 m, 3 m, 6 m, and 9 m (2.5 ft, 10 ft, 20 ft and 30 ft) from the right corner of the test pillar along the crosscut side. Profiles E-2.5, E-10, E-20, and E-30 were taken at distances of 0.75 m, 3 m, 6 m, and 9 m (2.5 ft, 10 ft, 20 ft, and 30 ft) from the right corner of the test pillar along the entry side.

Rib displacement comparison

The total rib displacements at each anchor of the MPBXs (Figure 4) were reduced from the measured displacements of the anchors of the MPBXs, as follows:

$$RD_i = AD_o - AD_i \qquad \textit{Equation 13}$$

where RD_i is the total rib displacement at anchor-i, AD_o is the measured displacement of the deepest anchor of the MPBX, and AD_i is the measured displacement of anchor-i.

It was reported that the MPBXs' rib anchors were repaired and reset prior to the reduction of the test pillar (pre-cut step). Therefore, the measured rib displacements during pillar reduction steps are the change of the rib displacement from the pre-cut step. Figure 6 shows the measured change in rib displacement at cut-7 (solid circles) for selected locations: X-10, X-20, X-30, E-10, E-20, and E-30 (see Figure 4 for locations of the profiles). The total and change in rib displacement at cut-7 were calculated by the model and illustrated in Figure 6 by dashed and solid lines, respectively.

The measured and model rib displacements at cut-7 show similar exponential decay behaviors (Figure 6). Both show a displacement decay interval (rib softening depth "DOS") of 2 m to 3 m (6.7 ft to 10 ft). The measured rib displacements at the entry side of the test pillar are about 10 mm (0.4 in) greater than that at the crosscut side. This anisotropic behavior of the measured rib displacements is a result of orienting the entries at the test site parallel to the face cleats. The rib displacements obtained by the model show similar anisotropic behavior, especially for a distance of 3 m (10 ft) from the right corner of the test pillar; the model rib displacement at location E-10 was about 20 mm (0.8 in) more than the rib displacement al location X-10. The model shows that the anisotropy of rib displacement becomes less pronounced toward the mid-length and mid-width of the test pillar; the model rib displacement at location E-30 was about 10 mm (0.8 in) more than the rib displacement al location X-30.

Vertical stress comparison

The measured total vertical stresses at each cut of pillar reduction were calculated by adding an average development stress of 7.21 MPa (1045 psi) to the measured changes in the vertical stresses. Figure 7 shows total vertical stress in test pillar A at cut-7 illustrated by solid circles. It shows total vertical stresses for selected locations: X-2.5, X-10, X-30, E-2.5, E-10, and E-30 (see Figure 3). Unlike the rib displacement, the anisotropic effect of the face cleat was less pronounced for the vertical stress at both the crosscut and entry profiles, especially for the first 4 m (12 ft) of pillar rib.

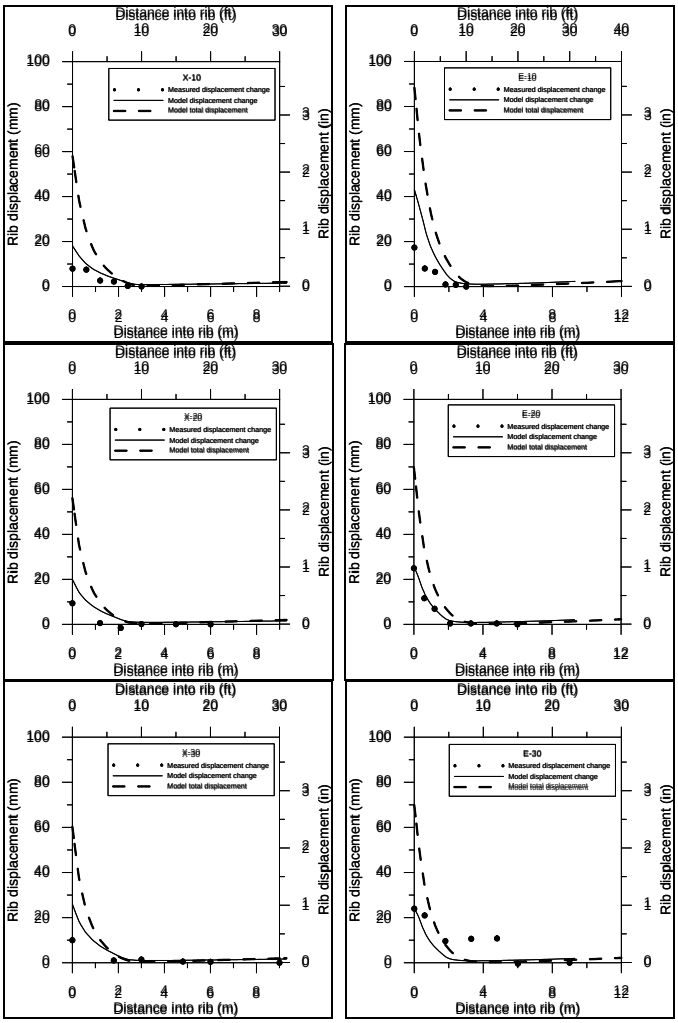

Figure 6. Rib displacement profiles of test pillar A at cut-7. Measured and model change in rib displacements are illustrated by solid circles and solid lines, respectively. The model total rib displacements are illustrated dashed lines.

The model total vertical stresses at cut-7 are illustrated by solid lines in Figure 7. The measured total vertical stresses at pillar corner, within a distance of 2 m (6 ft) of the test pillar corner, are greater than those obtained by the model. The measured average vertical stress at the corner of the test pillar is about 10 MPa (1,450 psi), which is about 75% of the intact strength of the coal material. This level of vertical stress could be too high, especially for the reported sloughing observed at the test site. The model prediction for the vertical stresses at the corner of the test pillar could be more realistic where it changes from zero to about 5 MPa (725 psi). Vertical stress profile E-2.5 showed good agreement between field and model, except in the first 2 m (6 ft) of the profile.

Profiles X-10 and E-10 show unrealistically low measured vertical stress at 3 m (9 ft). Ignoring this single data point, the vertical stress profiles X-10 and E-10 show a good match between the field and model.

Distant from the test pillar corner, the best match between the model and field was found near the mid-length and mid-width of the

test pillar, i.e., vertical stresses profiles X-30 and E-30. The model successfully predicted the location of the peak vertical stress at those profiles, but it underestimated the value of the peak vertical stress by about 2 to 7 MPa (290 to 1,015 psi).

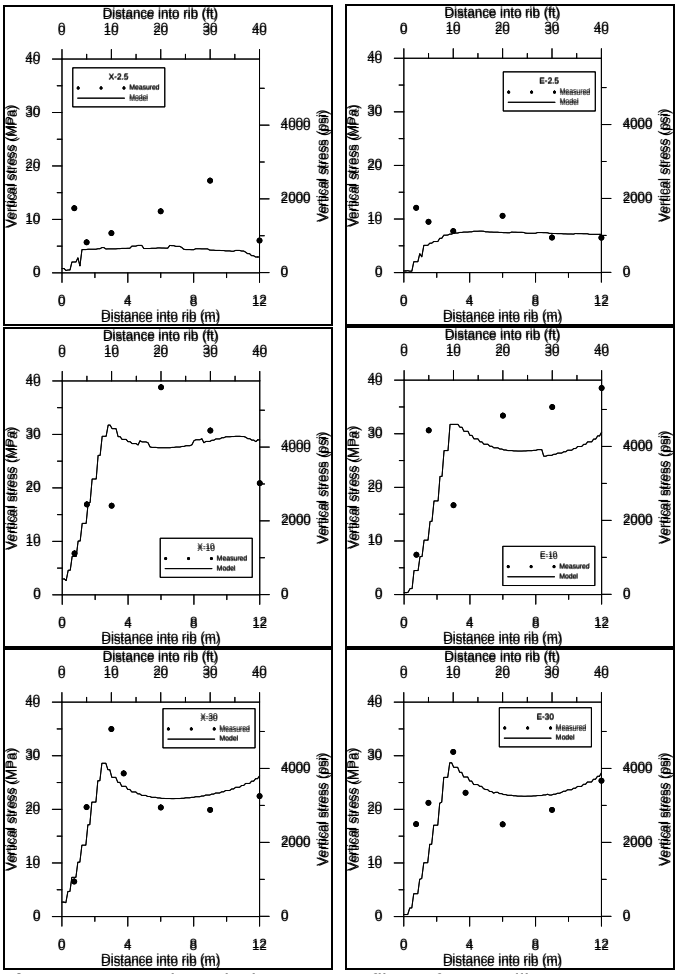

Figure 7. Total vertical stress profiles of test pillar A at cut-7. Measured and model vertical stresses are illustrated by solid circles and solid lines, respectively.

CONCLUSIONS

In this paper, researchers from the National Institute for Occupational Safety and Health (NIOSH) successfully improved and calibrated the coal-mass model. Rib failure incidents can be can be substantially reduced or even eliminated by adopting calibrated numerical model-based coal rib design approach. The orientation of face cleat with respect to driving direction was integrated successfully in the coal-mass model. The anisotropic effect of face cleats on the rib displacement was successfully modeled.

The controlling parameters (dimensionless coal-mass scale and fracture strains) of the coal-mass model were calibrated using a published case of a coal pillar strength study. The calibrated coal-mass scale is 30, and the calibrated fracture plastic shear and tensile strains are 3.25% and 0.325%, respectively. The current and previous calibration studies for different coal seams show that the coal-mass scale (CMS) varies from 20 to 35, and the fracture plastic shear strain varies from 2.75% to 3.75%.

Currently, NIOSH is conducting five in situ instrumentation sites in both longwall and room-and-pillar mines to further calibrate the coal-mass model.

DISCLAIMER

The findings and conclusions in this paper are those of the authors and do not necessarily represent the views of the National Institute for Occupational Safety and Health (NIOSH).

REFERENCES

1. Alejano, L. R. and Alonso, E., 2005, “Considerations of the dilatancy angle in rocks and rock masses,” International Journal of Rock Mechanics and Mining Sciences, Vol. 42, No. 4, pp. 481–507.

2. Colwell, M. G. and Mark, C., 2005, “Analysis and design of rib support (ADRS) – A rib support design methodology for Australian collieries,” Proceedings of the 24th International Conference on Ground Control in Mining, Morgantown, WV, University of West Virginia, pp. 12-22.

3. Esterhuizen, G.S., 2017, Personal communication.

4. Fang, Z., and Harrison, J.P., 2002, “Development of a local degradation approach to the modeling of brittle fracture of heterogeneous rocks,” *International Journal of Rock Mechanics and Mining Sciences*, Vol. 39, No. 4, pp. 443–457.

5. Gauna, M., and Mark, C., 2010, “Protecting underground coal miners from rib falls,” *Proceedings of the 30th International Conference on Ground Control in Mining*, Morgantown, WV, University of West Virginia, pp. 126–134.

6. Hoek, E., Carranza-Torres, C., and Corkum, B., 2002 “Hoek-Brown Failure Criterion – 2002 Edition” 5th North American Rock Mechanics Symposium and 17th Tunneling Association of Canada Conference, Toronto, Canada, Vol.1, pp. 267–271.

7. Holmes, P., 1981. “Relations between geology and the stability of faces and roadways in the Barnsley Seam,” Developments in Geotechnical Engineering, Vol. 32, 1981, pp 118–122.

8. Itasca Consulting Group, Inc. (2016). FLAC3D - Fast Lagrangian Analysis of Continua in Three-Dimensions, Ver. 6.0. Minneapolis: Itasca.

9. Liu, H., Sang, S., Xue, J., Wang, G., Xu, H., Ren, B., Liu, C., and Liu, S., 2016, “Characteristics of an in situ stress field and its control on coal fractures and coal permeability in the Gucheng block, southern Qinshui Basin, China,” Journal of Natural Gas Science & Engineering.

10. Mohamed, K., Murphy, M., Lawson, H., and Klemetti, T, 2015a, “Analysis of the current rib support practices and techniques in U.S. coal mines,” Proceedings of the 34th International Conference on Ground Control in Mining, Morgantown, WV, University of West Virginia, pp. 83–96.

11. Mohamed, K.M., Tulu, I.B., and Klemetti, T., 2015b, “Numerical Simulation of Deformation and Failure Process of Coal-Mass,” Proceedings of the 49th US Rock Mechanics/Geomechanics Symposium, Alexandria, VA, American Rock Mechanics Association.

12. Mohamed, K., Tulu, B., Murphy, M., 2016, “Numerical model calibration for simulating coal ribs,” Proceedings of the 35th International Conference on Ground Control in Mining. Morgantown, WV, University of West Virginia, pp. 289–298.

13. Salamon M.D.G., 1990, “Mechanics of Caving in Longwall Coal Mining,” Proceedings of the 31st U.S. Symposium on rock mechanics, Colorado School of Mines, Golden, CO, pp 161-168.

14. Sears, M.M, Rusnak, J., Van Dyke, M., Rashed G., Mohamed, K., and Sloan, M., 2017, “Coal Rib Response during Bench Mining: A Case Study,” Proceedings of the 36th International Conference on Ground Control in Mining, Morgantown, WV, University of West Virginia, pp. 67–75.

15. Wang, F.D., Skelly, W.A., and Wolgamott J., 1976, “In situ Coal Pillar Strength Study,” U.S. Department of Interior Bureau of Mines, Excavation Engineering and Earth Mechanics Institute, Colorado School of Mines, Final Report on Contract No. H0242022.

16. Zhang, P., Mohamed, K.M., Tulu, I.B., and Trackemas, J., 2017, “Coal Rib Failure and Support in Longwall Gate Entries,” Proceedings of the 51th US Rock Mechanics/Geomechanics Symposium, Alexandria, VA: American Rock Mechanics Association.